

Configurational Preferences of Arylamide α -Helix Mimetics via Alchemical Free Energy Calculations of Relative Binding Affinities

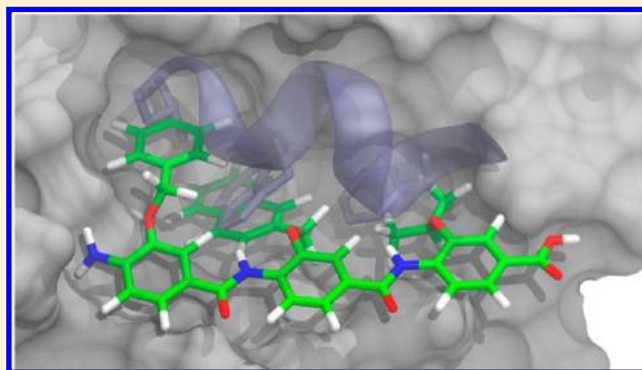
Jonathan C. Fuller,^{†,‡,§} Richard M. Jackson,[†] and Michael R. Shirts^{*,‡}

[†]Institute of Molecular and Cellular Biology and Astbury Centre for Structural Molecular Biology, University of Leeds, Leeds, LS2 9JT, United Kingdom

[‡]Department of Chemical Engineering, University of Virginia, Charlottesville, Virginia 22904-4071, United States

S Supporting Information

ABSTRACT: We use molecular docking and free energy calculations to estimate the relative free energy of binding of six arylamide compounds designed to inhibit the *h*DM2–p53 interaction. We show that using docking methods to predict or rank the binding affinity of a series of arylamide inhibitors of the *h*DM2–p53 interaction is problematic. However, using free energy calculations, we show that we can achieve levels of accuracy that can guide the development of novel arylamide compounds. We perform alchemical free energy calculations using the Desmond molecular dynamics package with the same arylamide inhibitors of the *h*DM2–p53 system and illustrate the challenges of performing accurate free energy calculations for realistic systems. To our knowledge, these are the first calculations for inhibitors of the *h*DM2 system that employ a full treatment of statistical mechanics including explicit water representation and full protein flexibility. We show that mutating three functional groups in a single transformation can be more efficient than mutating the groups one by one if proper intermediates are used. We also show that Hamiltonian exchanges can improve the efficiency of the calculation compared to standard alchemical methods, with a novel use of the phase space overlap to monitor sampling extent. We show that, despite sampling limitations, this approach can achieve levels of accuracy sufficient to bias further inhibitor modification toward binding, and identifies antiparallel configurations as stable or more stable than the parallel configurations that are typically considered.



INTRODUCTION

Free energy calculations have long been key tools of computational chemistry, with potentially transformative potential if made sufficiently fast and simple. For example, the ability to rapidly calculate the binding affinity of a ligand for a protein of interest would bring about a paradigm shift in the rational design of compounds in drug discovery efforts. Free energy methods can potentially also predict solubility and membrane permeability, physiochemical properties necessary to predict prospective drugs. In this study, we investigate both docking and recently developed free energy calculation techniques in order to rationalize binding affinities of novel arylamide compounds designed to inhibit the *h*DM2–p53 interaction.¹ Inhibition of the *h*DM2–p53 complex is of great interest in drug discovery due to its involvement in the regulation of apoptosis in cancer cells.² We perform free energy calculations of arylamide inhibitors of the *h*DM2–p53 interaction and illustrate that we can determine free energies of binding with usable levels of accuracy for guiding synthesis of novel *h*DM2–p53 inhibitors with enhanced binding affinity, as well as illustrating that docking of these molecules is not particularly useful to rationalize affinity. The arylamide compounds that inhibit *h*DM2 in this study are foldamer

compounds that take inspiration from oligomeric molecules with well-defined 3D structures such as α -helices. Like other heteropolymers such as proteins and RNA, foldamers can have well-defined secondary and tertiary structure.^{3,4}

The *h*DM2–p53 system is of significant biological and medicinal interest since the interaction has been shown to be involved in the control of apoptosis. Inhibiting this interaction could therefore be used to treat various types of cancers.^{2,5} Because of this therapeutic significance, several different methods for estimating binding affinity have been applied to a variety of compounds designed to inhibit the interaction. Molecular docking is the computationally cheapest way to investigate binding affinity and provide structural information about the bound complex, though in most cases docking scores have been shown not to correlate to binding affinity.⁶

In one study, which focused on synthesis and characterization of a diverse selection of arylamide compounds designed to inhibit the *h*DM2–p53 interaction, a very simple docking method was applied in order to gain insight into the structural

Received: September 19, 2011

Revised: June 4, 2012

Published: August 27, 2012

features of the *h*DM2–arylamide interaction.⁷ However, Shaginian et al. do not explicitly state the parameters that they used to dock their arylamide compound into the *h*DM2 binding site, or the optimization procedure that they applied after docking. Furthermore, Shaginian et al. reported only a single possible conformation and made no attempt to extrapolate their docking results to calculate the binding affinity for the different arylamide compounds investigated.⁷ In previous work, we addressed some of the deficiencies described above in the docking approach of Shaginian et al. by using increased sampling, investigating 150 possible binding modes, and analyzing the conformational degrees of freedom of the arylamide compound using extensive molecular dynamics simulation.⁸ We highlighted evidence for two classes of binding modes, antiparallel and parallel, of which only the parallel binding mode was identified and analyzed by Shaginian et al.⁷ As one of the goals of the present study, we assess the Autodock scoring function for its ability to determine the binding free energy of the arylamide compounds to *h*DM2. However, we also want to use more quantitative methods for determining *h*DM2 inhibitor binding affinities, specifically “alchemical” free energy calculations.^{9–16} In this paper, we use a number of recent improvements to free energy techniques in order to obtain free energies of binding for the *h*DM2 arylamide system with as high accuracy and efficiency as possible.

A number of recent simulation improvements have been proposed for improving the accuracy and reliability of free energy calculations and understanding the nature of variability in such calculations. For example, it has been shown that the charge model used to assign atomic partial charges and the water model used can significantly affect the results of free energy calculations.^{17,18} Mobley et al. shed light on the use of different charge calculation techniques used for hydration free energy calculations, indicating that standard charge calculation methods tend to affect the results at a level of around 1 kcal mol^{−1} rms error.¹⁷ Different water models can affect the calculated free energy of hydration of small molecules using the OPLS-AA force field. However, variation in the solvation free energies between water models is relatively small, with SPC/E and TIP4P-Ew giving the largest variation (greater than 0.6 kcal mol^{−1}) from experiment and TIP3P in close agreement (less than 0.25 kcal mol^{−1} difference to experiment) with TIP4P, SPC, and a modified TIP3P water model ranging in between those values.¹⁸ In this study, we used the AM1BCC charge calculation method and the TIP3P water model.

Efficient molecular simulation invariably requires use of cutoffs or otherwise truncated potentials to facilitate calculating the system’s properties. Inconsistent use of truncations can adversely affect the calculated free energy, but proper use of PME or dispersion corrections can improve the consistency of free energy calculations.¹⁸ Analytic dispersion corrections to correct for the pressure and energy of bulk fluids are frequently applied to larger nonisotropic systems such as solvated proteins. Recent work has found that these assumptions are not applicable to nonisotropic systems.¹⁹ For example, different choices of cutoff in the absence of an anisotropic dispersion correction can cause differences in the free energy of ligand binding between 0.5 and 2 kcal mol^{−1}, motivating our use of such anisotropic corrections here.¹⁹

Replica exchange techniques, like those used in this work, have recently been studied as a method of improving sampling.^{11,20–31} Traditionally, replica exchange has been

applied to replicas of the simulation system over a ladder of different temperatures. In free energy calculations, the same bookkeeping system of exchanges between intermediates is used but simulations are performed at a variety of intermediate λ values as required for standard free energy calculations. Exchanges are made subject to a criteria defined by detailed balance, allowing swaps between adjacent λ values, analogous to the temperature replica exchange (T-REMD) process.²⁰ Comparison of replica exchange thermodynamic integration (RETI) to standard FEP, WHAM, and several variants of TI show that RETI performs better than the other methods to determine the free energy of methane hydration.^{11,31,32} Replica exchange methods are relatively straightforward to implement, and many simulation code bases such as Desmond include them as standard options.³³ Regions of phase space with good overlap between sampled states will have high rates of acceptance of proposed exchanges, whereas regions of phase space with low overlap will have low rates of acceptance of the exchanges.

In addition to the technical improvements described above, we use in our free energy calculations lessons learned from studies of other foldamers interacting with *h*DM2 that can help us understand potential issues with arylamide binding. One such class of foldamers studied in complex with *h*DM2 is the β -peptide family. β -Peptides are synthetically produced from β -amino acids, which have an additional backbone carbon and have their amino group bonded to this β -carbon instead of the α -carbon. β -Peptides have pharmaceutical advantages over traditional optimized peptides including their stability in the cell and decreased immune response. Michel and co-workers applied a de novo design strategy to a previously discovered β -peptide and identified 50 candidate side-chain replacements from 10 000 structures with aromatic and nonaromatic heterocycles substituted.³⁴ Binding free energies were then calculated with MC/FEP calculations for the peptides using the OPLS/AA force field and TIP4P water. A selection of eight of the most synthetically accessible compounds was re-evaluated using a second, more accurate round of MC/FEP. The study revealed novel β -peptides with experimental affinity improved from 204 nM in the starting compound to 27.6 nM in the case of the β -peptide with the best affinity for *h*DM2.³⁴ This study also produced high-affinity β -peptides that target the related *h*DMX interaction with differing levels of specificity between *h*DM2 and *h*DMX.³⁴ As a result of these researches, Michel et al. achieved accuracies that allowed them to guide synthesis of new compounds in their calculations.³⁴

Previous to the study presented in this article we have carried out a detailed analysis of the behavior of an arylamide in the *h*DM2 binding pocket, a necessary prerequisite to performing well-converged free energy calculations.⁸ We showed that the GAFF and Autodock potentials did not accurately describe the known behavior of the arylamide ArNH and ArCO dihedral angles from NMR NOESY spectra, but could be modified to correctly represent this behavior. Through molecular dynamics simulations of the arylamide compound in the *h*DM2 binding pocket, we showed that some starting configurations obtained from molecular docking begin to converge on the time scale of 20 ns simulations; however, several did not. Those configurations that do not converge to the same region of the binding site are sampling disjoint regions of phase space, which is an important consideration when attempting to converge free energy calculations.³⁵

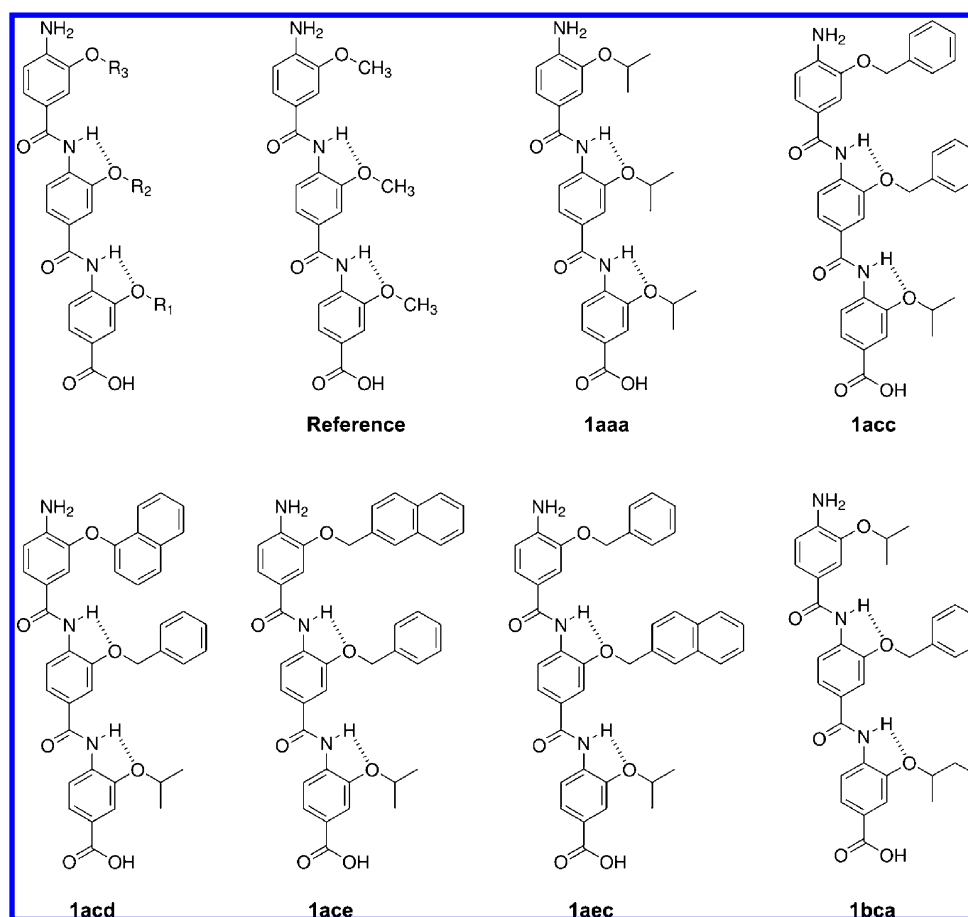


Figure 1. Structure to which all compounds are mutated alchemically is labeled as “Reference” and the experimentally synthesized and tested arylamide compounds investigated in this work are labeled 1aaa through 1bca.¹

Inspired by the successful application of free energy calculations to the β -peptides described above, we calculate the binding free energy of arylamide compounds to *hDM2*, using alchemical free energy calculations, fully flexible protein simulations, and an explicit solvent model. The calculations presented in this paper appear to be the first alchemical free energy calculations with fully flexible protein and explicit water of any *hDM2* ligands, and additionally compare the effectiveness of these methods with cheaper molecular docking methodologies. We build on recent previous work using computational docking of compounds and molecular dynamics simulations of complexes to provide high-quality starting structures spanning a large range of conformations.⁸ In this study, we perform free energy calculations for six arylamide compounds using multiple configurations from our previous study to aid convergence and report levels of accuracy sufficient to help guide design of novel arylamide side chains.

EXPERIMENTAL METHODS

Using Autodock To Generate *hDM2*–Arylamide Conformations. We used Autodock 4.2.1^{36,37} to dock the arylamide compounds shown in Figure 1 into the *hDM2* binding site, generating initial conformations for performing relative binding alchemical free energy calculations between these compounds and the common substructure compound (labeled “Reference”) shown in Figure 1. Previously, we performed docking of compound 1aec in order to evaluate the performance of Autodock at structure generation where we

developed the parameters used here.⁸ Two rounds of docking using Autodock^{36,37} were performed in the current study to assess whether a less computationally intensive set of parameters can generate conformations sampling the conformational degrees of freedom to the same extent. Importantly, to obtain converged distributions, both strategies used significantly more energy evaluations than is the default for Autodock.

The first round of docking calculations used Autodock to produce 300 docked conformations with a maximum of 25 million evaluations for 27 000 generations with population size 300 using the compounds detailed in Figure 1. The second round of docking produced 600 docked conformations, each using 250 million evaluations for 64 000 generations of population size 600. Random number seeds were generated from the Autodock process ID and the current system time. The protein structure was derived from the structure of *hDM2* bound to a high-affinity p53 helix (1T4F), with all water molecules removed, protonation states manually assigned, and the high-affinity p53 helix removed from the coordinates. A grid centered on [13.119, 18.969, 10.941] was used with spacing of 0.375 Å and 52, 58, and 48 points in the *x*, *y*, and *z* directions.

Free Energy Calculations with Desmond. Equilibration. All simulations performed were subjected to a six-step equilibration procedure to ensure that the system was in a suitable equilibrium state before the free energy calculations were carried out. The procedure is listed in full in the Supporting Information section “Six step equilibration procedure”.

Free Energy Calculation. For all free energy calculations, we performed 5 ns of molecular dynamics simulation at each value of λ . The Martyna–Tobias–Tuckerman–Klein constant pressure and temperature method was used with a coupling time of 2.0 ps.³⁸ The reference temperature was 300 K, with two discrete updates to Nose–Hoover barostat variables per time step and with a barostat time constant of 1.0 ps.³⁹

Because Hamiltonian replica exchange molecular dynamics (H-REMD) will result in better sampling than simulations of the same set of Hamiltonians performed without exchange,^{11,20–29,31} the majority of simulations were performed using a Hamiltonian replica exchange methodology described below. However, to assess the utility of H-REMD in this system, selected free energy calculations without H-REMD were also performed. Both sets of simulations used the same simulation parameters listed in the final (step 6) equilibration stage, except as noted.

Hamiltonian Replica Exchange Molecular Dynamics (H-REMD). Replica exchange techniques with exchange of Hamiltonian should allow enhanced sampling of configurations, with decreased correlation between samples. Specifically, when the dihedral potential and Lennard-Jones interaction energies of the side chains of the target state gradually change to those of the reference state as a function of λ , the correlation times of these dihedral angles should be significantly reduced, as the reference state interactions for the side chains are turned off, so that the side chains do not interact with the other atoms. The increased flexibility of side chains in the reference state should allow for easier convergence of these dihedral angles to the equilibrium distribution. This process will generally reduce overall structural correlation times, since these small side chains should be freer to rotate than larger, more constrained side chains. When using replica exchange, if converged side-chain dynamics are not observed, then the alternative orientations of these dihedral angles must be included as part of the initial configurational ensemble to fully capture the extent of configurational sampling of the ligand.³⁵

In this study, replica exchange calculations with 24 replicas with intermediate states described in Table 1 were carried out for 5 ns with exchanges between neighboring replicas attempted every 12 ps. Equation 1 was used to calculate the acceptance of exchanges.

$$Q = (\beta_1 U_{11} + \beta_2 U_{22} - \beta_1 U_{12} - \beta_2 U_{21}) \\ + (\beta_1 P_1 - \beta_2 P_2)(V_1 - V_2) \quad (1)$$

In eq 1, U_{ij} is the potential energy of replica i under the Hamiltonian of replica j , P_i is the instantaneous pressure of replica i , V_i is the volume of replica i , and β_i is the inverse temperature of the i th replica scaled by k_B . Exchanges are accepted if $Q > 0$. When Q is between 0 and -20 , the exchanges are made with the criteria $\text{rand}(N) < \exp(Q)$, where $\text{rand}(N)$ is a random number in the range 0–1. If $Q < -20$, exchanges are rejected. This truncation introduces a very small but nonzero probability of deviation from the true ensemble since one would expect $Q < -20$ to occur approximately once every 485 million swaps. This deviation should be negligible on the time scale that we simulate since swaps are only attempted 10 000 times. In order to compare the Hamiltonian replica exchange method to simulations without exchange, we also used 24 independent simulations with standard molecular dynamics with the same simulation parameters as the Hamiltonian replica exchange calculations.

Table 1. Parameter Scaling for Different Values of λ in the 24-Window Schedule Used in the Final Simulations

	charge A	charge B	bonded A	bonded B	vdW A	vdW B
0	1.0	0.0	1.0	0.0	1.0	0.0
1	0.889	0.0	1.0	0.076	1.0	0.067
2	0.778	0.0	1.0	0.143	1.0	0.119
3	0.667	0.0	1.0	0.214	1.0	0.158
4	0.556	0.0	1.0	0.286	1.0	0.190
5	0.444	0.0	1.0	0.357	1.0	0.218
6	0.333	0.0	1.0	0.429	1.0	0.247
7	0.222	0.0	1.0	0.5	1.0	0.282
8	0.111	0.0	1.0	0.571	1.0	0.325
9	0.0	0.0	1.0	0.643	1.0	0.382
10	0.0	0.0	0.929	0.714	0.827	0.456
11	0.0	0.0	0.857	0.786	0.675	0.553
12	0.0	0.0	0.786	0.857	0.553	0.675
13	0.0	0.0	0.714	0.929	0.456	0.827
14	0.0	0.0	0.643	1.0	0.382	1.0
15	0.0	0.111	0.571	1.0	0.325	1.0
16	0.0	0.222	0.5	1.0	0.282	1.0
17	0.0	0.333	0.429	1.0	0.247	1.0
18	0.0	0.444	0.357	1.0	0.218	1.0
19	0.0	0.556	0.286	1.0	0.190	1.0
20	0.0	0.667	0.214	1.0	0.158	1.0
21	0.0	0.778	0.143	1.0	0.119	1.0
22	0.0	0.889	0.071	1.0	0.067	1.0
23	0.0	1.0	0.0	1.0	0.0	1.0

Choice of λ States. We used the dual topology approach implemented in Desmond to perform our alchemical transformations. Alchemical free energy calculations were performed using $\alpha = 0.5$ for the soft core potential.^{18,40} We used 24 windows with charge, bonded, and van der Waals parameters, changing according to the schedule shown in Table 1 and generated by default in Desmond. For comparison, we also used λ parameters for 12 windows with a similar scheme for switching the parameters (Supporting Information, Table S1) and also a scheme whereby we first scaled electrostatic interactions, then van der Waals followed by bonded interactions using 40 windows (Supporting Information, Table S2).

Nonbonded Interactions. Short-range van der Waals and electrostatic interactions used a cutoff at 9 Å and used a lazy migration radius of 10 Å. Lennard-Jones parameters were cutoff at 9 Å. Far electrostatic interactions were calculated using PME on a cubic FFT grid with 32 points in each direction, PME interpolation order 4, and Ewald sigma coefficient 2.17. We used the soft-core potential detailed in eq 2 as implemented in Desmond for removing Lennard-Jones sites.

$$U_{ij}^{\text{vdW}}(r_{ij}; \lambda) = 4\epsilon_{ij}\lambda \left\{ \frac{1}{\left[\alpha_{\text{vdW}}(1 - \lambda)^2 + \left(\frac{r_{ij}}{\sigma_{ij}} \right)^6 \right]^2} - \frac{1}{\left[\alpha_{\text{vdW}}(1 - \lambda)^2 + \left(\frac{r_{ij}}{\sigma_{ij}} \right)^6 \right]} \right\} \quad (2)$$

In the above equation for the van der Waals potential U_{ij} , α_{vdW} is the scaling parameter, λ is the order parameter along which the mutation is performed, ε_{ij} is the depth of the well at the minimum of the van der Waals function, σ_{ij} is the point at which the van der Waals energy of the uncoupled state is zero, and r_{ij} is the distance between atoms i and j . It has been shown previously that it is more efficient to use the soft-core potential $(1 - \lambda)$ rather than $(1 - \lambda)^2$.^{18,40} However, this has not yet been implemented in the Desmond code.³³

Global Cell. Simulations were partitioned such that each used 8 CPUs for each λ state, with two partitions in each axis direction. The rounded clone policy was used, with an estimated one atom per particle array voxel. The clone radius was set to 11 Å, significantly larger than the default 5.000 000 01 Å, in order to allow multiple functional group mutation; this was necessary for the particular multiple site mutations performed in this study. The choice of a larger clone radius adversely affects the simulation performance, because a water box that accommodates the larger clone radius must be used. Due to implementation details of the Desmond free energy calculation algorithms, the clone radius had to be extended for the single process three mutation simulations, which required addition of more water molecules, thus increasing simulation time somewhat, but this is an implementation issue that could be corrected and is not necessarily present in other molecular simulation codes.

Calculation of Free Energy Using Bennett Acceptance Ratio. We modified the Bennett acceptance ratio script included with Desmond to create 200 bootstrap data sets by resampling with replacement from the computed energies. The free energy between all pairs of neighboring states is calculated according to the Bennett acceptance ratio for each of these resampled data sets. The total free energy to change from state $\lambda = 0$ to $\lambda = 1$ is then the sum of the free energies from each of the windows between state $\lambda = 0$ and $\lambda = 1$. Initial inspection of the Bennett acceptance ratio scripts in Desmond suggest that a bootstrapping method is used to calculate the variance; however, closer inspection reveals that a block average is used instead, which has been communicated to the Desmond developers for correction in future releases. We implemented a bootstrap calculation of statistical error that is described in detail in the Supporting Information section "Calculation of errors".

Calculating a Single Free Energy from Simulations of Multiple Configurations. We combined multiple simulations of the same hDM2 arylamide with different starting conformations using the technique of exponential summation of the free energies. The technique is rigorous for independent conformational ensembles. In one example of this technique, Mobley et al. used a simple exponential summation to combine the results from two simulations using different starting conformations for which they had computed "effective" binding free energies: ΔG_1^0 and ΔG_2^0 .³⁵

$$\Delta G^0 = -\beta^{-1} \ln[e^{(-\beta\Delta G_1^0)} + e^{(-\beta\Delta G_2^0)}] \quad (3)$$

Here $\beta = (k_B T)^{-1}$, where k_B is the Boltzmann constant and T is the temperature. The equation can be trivially generalized to take into account the results from N simulations for any case where the simulations are sampling disjoint regions of phase space:

$$\Delta G^0 = -\beta^{-1} \ln[e^{(-\beta\Delta G_1^0)} + e^{(-\beta\Delta G_2^0)} + e^{(-\beta\Delta G_3^0)} + \dots + e^{(-\beta\Delta G_N^0)}] \quad (4)$$

The assumption that simulations are sampling disjoint regions of phase space is certainly true for the case of parallel and antiparallel arylamide conformations. We used conformational convergence data described in our previous study to select a second antiparallel starting conformation that also samples a disjoint region of phase space.⁸ In fact, this decomposition should work regardless of whether there is mixing between the configurations, as long as the relative probabilities are correct. With this caveat, the resulting free energy is correct, although the individual state free energies are not meaningful.

Anisotropic Dispersion Correction. We applied anisotropic dispersion corrections to the calculations in order to eliminate the effect of cutoffs on the free energy calculations.¹⁹ Snapshots from each simulation were taken from the $\lambda = 0$ trajectories at intervals of 200 ps. The total potential energy of the system was calculated using the same parameters as described for the free energy calculations, with the only differences being the use of a Lennard-Jones cutoff value of 25 Å instead of 9 Å and the removal of the switched potential for the long-range calculations. The short-range Lennard-Jones energy is then subtracted to calculate an instantaneous long-range correction. A cutoff of 25 Å has been shown to be a reasonable parameter to account for long-range dispersion interactions in protein–ligand interactions in previous work.¹⁹ The energy difference between the standard cutoff and the long-range cutoff is determined for each of these samples and then combined using the Zwanzig relationship:

$$\Delta G = \frac{1}{\beta} \ln \langle e^{-\beta\Delta E} \rangle \quad (5)$$

The dispersion correction to the free energy calculations is calculated by using the thermodynamic cycle decoupling the ligand from the complex, and ligand from solution with short-range cutoffs to the same two transformations carried out with long-range cutoffs (see Figure 2).

Overlap Integrals. In Bennett's original derivation of his acceptance ratio method (BAR),⁴¹ he defined a formula for the estimated variance associated with a free energy measurement:

$$\sigma^2 = \frac{2}{n} \left[\left(\int \frac{2\rho_0\rho_1}{\rho_0 + \rho_1} dq^N \right)^{-1} - 1 \right] \quad (6)$$

Here ρ_0 and ρ_1 are the normalized probability densities of the configuration space of state 0 and state 1, respectively. The integral in eq 6 can be interpreted as the overlap between the two probability densities. Bennett showed that the minimum variance of a free energy calculation is proportional to the phase space overlap between two states.⁴¹

Following Bennett, we define the overlap $O(x_0, x_1)$ between two thermodynamic states as

$$\left(\frac{N\sigma^2}{x_0x_1 + 1} \right)^{-1} = \frac{O(x_0, x_1)}{x_0x_1} \quad (7)$$

where N is the total number of uncorrelated samples from both states, σ^2 is the variance, x_0 is the fraction of the samples in trajectory 0, and x_1 is the fraction of samples in trajectory 1. An overlap close to zero indicates that the two states sample from very different portions of phase space, whereas an overlap close

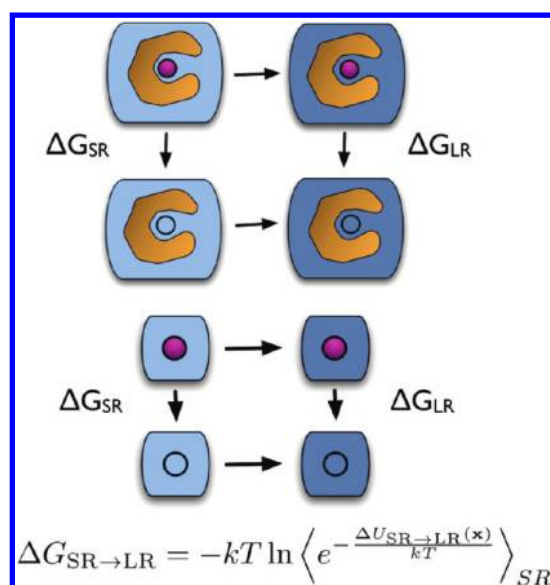


Figure 2. Components of the thermodynamic cycle used to apply anisotropic dispersion corrections to simulations performed with short-range (SR) cutoffs by reprocessing the trajectories using long-range (LR) cutoffs.¹⁹ The final correction to the binding free energy will be the difference between the complexed ligand and the solvated ligand long-range corrections to the free energy.

to one is the maximum and indicates two states sample from the same configurations in phase space. In the cases presented in this work, the samples all have x_0 equal to x_1 , and N is 9982 (samples taken every 1.002 ps from 5 ns of total simulation time) for H-REMD simulations and 9999 for non-H-REMD (samples taken every 1 ps from 5 ns of total simulation time) simulations. Whether or not the samples are correlated or uncorrelated will affect the total variance, but will not affect the overlap integral.

The statistical uncertainty of a calculation can be large because of either a small overlap or because of a small effective number of samples. The amount of overlap can allow us to determine whether it might be more efficient to increase the number of samples by running longer simulations or alternatively to increase the number of λ windows or readjust their spacing. In intervals where the overlap in a given window between λ values is low compared to the average overlap for the calculation, redistributing the λ states to sample more heavily in this region should help to increase the overlap, thus the rate of exchange in H-REMD, and thus the efficiency of the calculation.

Topology. A novel feature of this study is that, instead of making one change to a side chain at a time, we alter all three side chains in a single process. Conventional wisdom dictates that changing this many atoms at a time is statistically inefficient as it will lead to low overlap between states and requires many samples to converge the free energy of transformation. However, improved alchemical paths and methods have reached the point where the largest efficiency problem is likely the amount of time required for structural rearrangement of a protein, not the amount of time to sample the phase space differences between alchemical mutations.^{18,40} We mutate the side chains shown in Figure 1 (1aaa, 1acc, 1acd, 1ace, 1aec, 1bca) to the reference compound in a single process. In order to compare to a more traditional pathway where the mutations to a methyl functional group are

performed sequentially in three separate processes, we perform sequential transformations of the middle functional group (R_2), the N-terminal functional group (R_3), and, finally, the C-terminal functional group (R_1) to methyls. The free energy change of the total mutation is calculated using the thermodynamic cycle shown in Figure 3.

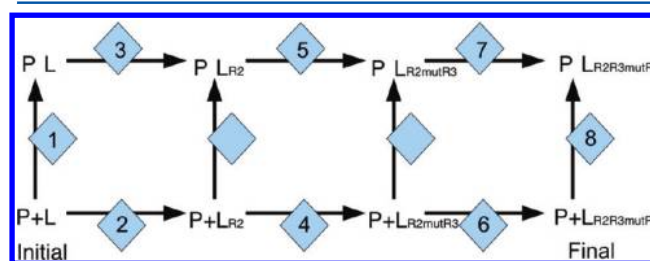


Figure 3. Thermodynamic cycle used to calculate the total free energy change of the entire process from the three sequential single mutations.

RESULTS

Generating Starting Conformations. Arylamide backbones are conformationally constrained by an intramolecular hydrogen bond between the ether oxygen and the amide hydrogen, but their side chains are flexible, resulting in a large variety of possible conformations that they can adopt in the *h*DM2 binding site. We use computational docking to generate likely conformations that can be used as starting points for molecular dynamics simulation. In a previous paper, we have identified putative models of compound 1aec bound to *h*DM2 that models remained stable in the *h*DM2 binding site over 20 ns of MD simulation.⁸ Here, we apply the same docking methodology to determine starting conformations for the remaining compounds shown in Figure 1. 600 docked conformations were generated using the expanded sampling parameter docking methodology discussed in the Experimental Methods. We show the structure (shown with atom type coloring in Figure 4) with the lowest rmsd compared to conformation 2, the largest low-energy cluster identified in our previous study, indicating close agreement between the previous and current docking calculations (shown colored green in Figure 4).⁸ We see that the newly generated

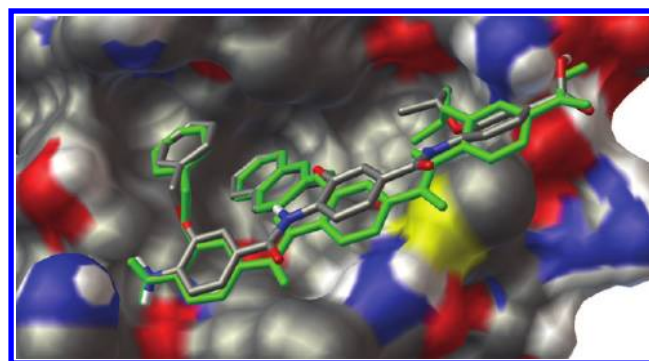


Figure 4. Reproducibility of the docking results shown by the close agreement between the two arylamide structures. Structure of a single conformation of compound 1aec from an Autodock run generating 600 conformations, shown in stick representation, with atoms colored by type compared to conformation 2 (green) as identified in previous work.⁸

conformation (shown with atom type coloring) is very similar to conformation 2 (shown in green), with rmsd between the two conformers of only 0.45 Å. The low rmsd between low-energy structures from the two independent docking calculations indicates that our sampling parameters give converged results between independent calculations.⁸ Further support for the suitability of the Autodock sampling parameters is given by the similarity in the distribution of Autodock scores observed for clusters of docked poses (shown in Figure 5),

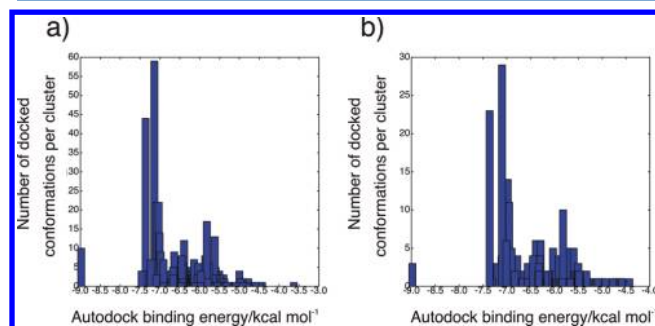


Figure 5. Autodock binding energy distributions for compound 1aec: (a) 600 conformations; (b) 300 conformations. Similar energy distributions of clusters are observed in each, indicating that the docking experiment with 300 docked conformations still samples the same low-energy regions. Generally, this suggests that enhanced sampling parameters (250 million evaluations and a population size of 64 000) are required to adequately sample the conformational space of these arylamide compounds, and that accepting fewer highly ranked conformations can provide adequate sampling.

indicating that similar lower conformations are reproducibly identified. In all cases, significantly more computationally expensive sampling parameters than the default Autodock parameters are required to dock arylamide compounds to reproducible conformations.

We next ask whether the Autodock scoring function is correlated to relative binding affinities for the six arylamide compounds in Figure 1. To test the Autodock scoring function, we used three measures as potential estimators of the binding affinity. The first is the average binding score, calculated from an exponential (Boltzmann) average of the scores for each of the Autodock conformations generated. The second is the energy of the low-energy cluster with the highest population (i.e., the energy of the tallest bar from the histograms in Figure 6). Finally, we use the most traditional method, the score of the lowest scoring conformer. The first two methods attempt to incorporate configurational averaging that is missing in standard docking in a physically meaningful way. A recent docking study by Illingworth et al. suggests that the largest low energy cluster is most useful for assessing the quality of docking results with Autodock, since an improvement in the methodology always results in an improvement of the rmsd relative to the crystal structure.⁴² We compared these three measures to the relative free energies derived from the experimentally determined IC_{50} data for the arylamide compounds, with results shown in Table 2 and Figure 7. Figure 8 shows the three best scoring docked conformations for each ligand demonstrating the range of conformations generated. Both parallel and antiparallel conformations are evident for all ligands. There is also significant diversity in the arrangements of the side chains relative to the hDM2 binding site within both parallel and antiparallel groups of conformations.

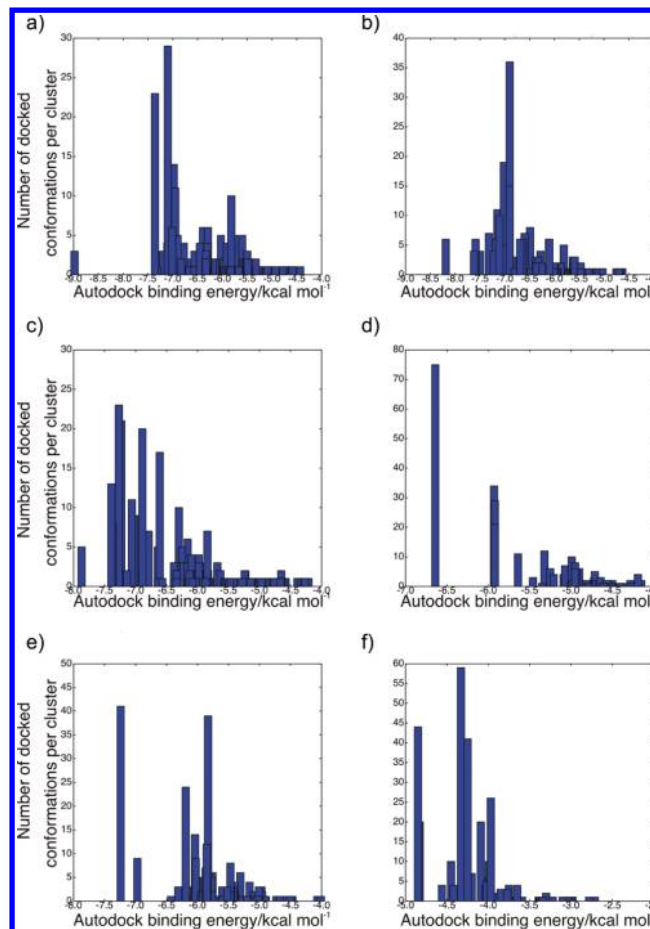


Figure 6. Distribution of Autodock binding energy scores for 300 docked arylamide conformations for compounds: (a) 1aec, (b) 1ace, (c) 1acd, (d) 1bca, (e) 1acc, and (f) 1aaa. Conformations generated using 250 million energy evaluations and a population size of 64 000.

Table 2. Binding Energy Relative to the Reference Compound Estimated from Experimental IC_{50} Compared to Autodock Relative Energies for the Largest Low-Energy Cluster, Lowest Energy Conformation, and the Exponential Average of Energies from All Docked Conformations

compd	exptl binding energy/kcal mol ⁻¹	Autodock largest cluster energy/kcal mol ⁻¹	Autodock lowest energy conformation/kcal mol ⁻¹	Autodock weighted av binding energy/kcal mol ⁻¹	alchemical free energy calculations/kcal mol ⁻¹
1aec	-1.37	-2.8	-4.13	-0.375	-1.84
1ace	-1.09	-2.6	-3.34	-1.583	-1.18
1acd	-0.85	-3	-3.02	-1.422	-2.16
1bca	-0.45	-2.25	-1.79	-0.662	-1.34
1acc	-0.40	-2.9	-2.39	-1.49	-1.46

Free Energy Calculations. We performed alchemical free energy calculations with the aim of correctly quantitatively ranking the binding affinity of different compounds.

Choice of λ Intermediates. Altering the number of and placement of λ intermediates allows us to minimize the calculated variance associated with each window between intermediates and thus minimize the variance in the total free energy calculation. λ intermediates should be placed such that the error associated with each window is approximately equal, because a single large error will increase the error of the entire

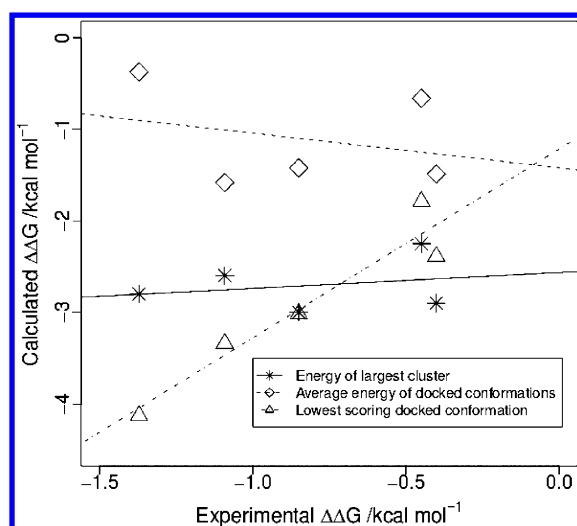


Figure 7. Calculated relative binding energy vs experimental relative binding energy for energy of the largest low-energy cluster as identified by Autodock (unbroken line and asterisks), exponentially averaged docked conformations from Autodock (dashed line and diamonds) and lowest energy conformation (dot-dashed line and triangles). R^2 for least-squares fits of the Boltzmann-averaged energy, low-energy cluster, and lowest energy are 0.08, 0.06, and 0.92, respectively.

calculation according to the square, since independent variances sum, not independent errors. In Figure 9, the bar for λ_i represents the error for the measurement of changing from λ_{i-1} to λ_i . When only 12 windows (Figure 9a, left) are used, the variance in the free energy calculated from each window is more than twice that when 24 windows are used (Figure 9a, right). Doubling the number of windows to 24 more than halves the magnitude of the individual errors, suggesting that 24 windows provide an appropriate balance between accuracy and computational tractability. For this specific case of spacing in 24 windows, the magnitude of the variance is within a factor of 5 between all windows. The list of intermediate states for each λ component is shown in Table 1 in the Experimental Methods section and Tables S2 and S3 in the Supporting Information.

Identifying specific windows that contribute significantly to the variance of the λ window would allow more finely spaced windows to be used for this part of the calculation, allowing the variances to be balanced more efficiently, resulting in a lower total calculation variance with fixed computational cost. We investigated different schedules sequentially switching off electrostatic interactions followed by van der Waals interactions and then bonded interactions before turning on the components in reverse sequence to obtain the final state.

While schedules in Figure 9a both switch off electrostatic interactions separately, the results in Figure 9b are generated by individually switching off the van der Waals interactions, then the bonded interactions, followed by turning on the bonded, then the van der Waals interactions and finally the Coulomb interactions of the mutant (full details in Table S2 in the Supporting Information). Since switching off the electrostatic interactions is the same in both the calculations performed in Figure 9a,b, it is not surprising that the variances are of the same magnitude. Switching off/on the van der Waals interactions alone is also reasonable in terms of the magnitude of the errors. However, altering the bonded parameters has a very large associated statistical error, apparently due to

complete decoupling of the bonded terms; thus, such transformations should be avoided.

Single Mutations versus Multiple Mutations. Previously we showed that it is desirable to simulate hDM2-ligand for longer than 5 ns in order to properly capture the sampling of certain dihedral angles of residues in the hDM2 binding pocket as well as dihedral angles in the arylamide compound.⁸ Thus, simulation strategies maximizing continuous long sampling simulations are likely to be beneficial. Analogously to mutation of amino acid side chains, we wish to “mutate” each of the functional groups that mimic amino acid side chains for the compounds in Figure 1 to the reference compound with methyl functional groups. It is possible to perform the mutation as a series of steps, mutating the first side chain in one simulation, the second side chain in a second simulation, and finally the third side chain in a third simulation, as shown in the thermodynamic cycle in Figure 3. However, it is also possible to mutate all three side chains in a single simulation. Performing the mutation of all three arylamide side chains to a common reference molecule in a single simulation has the potential to be more computationally efficient than performing three individual mutation simulations, since the simulation can be run for three times as long compared to performing three individual mutation simulations, at the cost of potentially lower phase space overlap for each mutation.

We assess the difference between performing a single process mutation of all three side chains and combining three stages of mutations via the thermodynamic cycle shown in Figure 3. We use this thermodynamic cycle to determine the free energy difference in binding of the total transformation from the sum of individual mutations, from state 1 to state 8:

$$\langle 1 \rangle - \langle 8 \rangle = [\langle 2 \rangle + \langle 4 \rangle + \langle 6 \rangle] - [\langle 3 \rangle + \langle 5 \rangle + \langle 7 \rangle] \quad (8)$$

The difference of only 0.7 kcal/mol between solvation simulations of the arylamide using the single-process mutation (-24.27 ± 0.26 kcal mol⁻¹) and the three-process mutation (-23.56 ± 0.36 kcal mol⁻¹) is small, indicating that both of these calculations are nearly converged to within statistical error, even though the three-process mutation used only one-third of the simulation time. We do note that a large difference of 3.8 kcal mol⁻¹ is observed in the calculated binding energy between the single-process mutation compared to the three-process mutation. This difference is due to a large difference in the results from the protein–ligand complex. The change in free energy of the complex for the single-process mutation is (-4.15 ± 0.22 kcal mol⁻¹) compared to that of the three-process mutation (-7.95 ± 0.30 kcal mol⁻¹), as seen in Table 3. Importantly, the phase space overlap between the states should be essentially the same for the decoupling simulations in solvent and in the complex. In both cases, the insertion process consists of the creation of a cavity, adding dispersion energy, and adding electrostatic energy. Although the energies of these processes differ depending on exactly what is being displaced, resulting in differences in free energy, the phase space overlap and thus the statistical variance are roughly the same, whether the insertion occurs in pure solvent or a mixed solvent/protein environment. This suggests that the difference is due primarily to conformational sampling problems in the complex rather than lack of phase space overlap in the single mutation process.

Hamiltonian Exchange versus Uncoupled Long Time Scale Simulations. Hamiltonian replica exchange in λ space was used as a method of enhanced sampling in order to

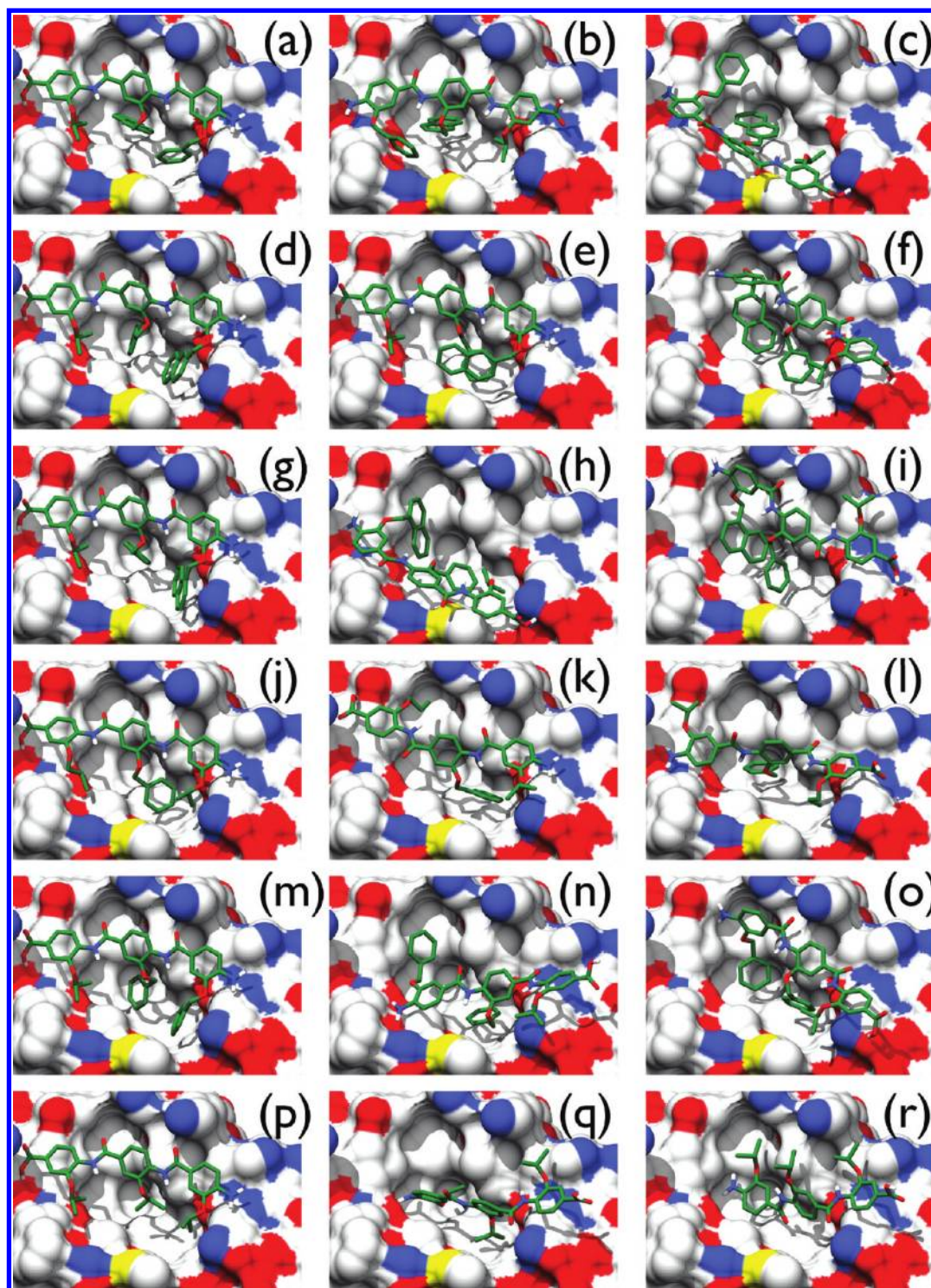


Figure 8. Highest scoring three poses from each complex are shown for illustrative purposes to convey the variety of starting conformations chosen. These poses were used as starting points for free energy calculations: (a–c) 1aec; (d–f) 1ace; (g–i) 1acd; (j–l) 1bca; (m–o) 1acc; and (p–r) 1aaa.

improve sampling of side-chain rotamer states that might be less accessible in standard simulations of several nanoseconds. Table 4 shows that in the case of the compound 1aec when conformer 2 is used, the results from H-REMD and non-H-REMD are within $0.5 \text{ kcal mol}^{-1}$, indicating good agreement between the two methods.

The exchange of replicas throughout the 5 ns of a simulation of conformation 2 of compound 1aec in complex is shown in Figure 10, where we can see that at least 10 exchanges occur

between all adjacent replicas, with many λ values participating in far more than 10 swaps. However, we note the limited number of swaps between replicas 12 and 13, meaning that the replica exchange chain is not mixing completely. This means that we are not getting the full benefit of allowing all side-chain states to explore the greater conformational freedom of the fully uncoupled states. Although sampling is almost certainly increased to some extent, improved replica exchange schema will be required to fully take advantage of Hamiltonian

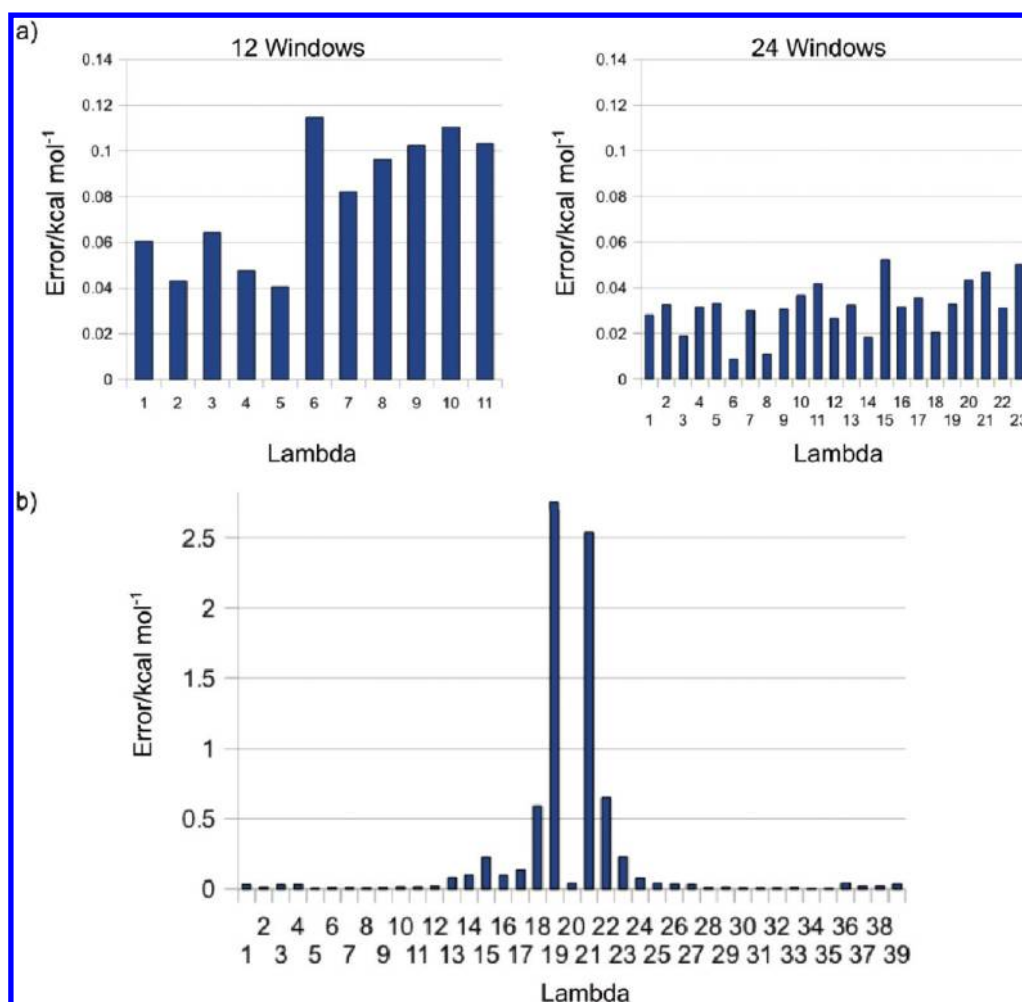


Figure 9. (a) Statistical uncertainty for simulation with 12 λ windows (left) and 24 λ windows (right). λ scaling is shown in Table 1 for 24 λ windows and in Table S1 in the Supporting Information for 12 λ windows. Uncertainty in free energy calculated at each window is balanced to within a factor of 5 in both cases, indicating an acceptably efficient placement of intermediates. (b) Error rate for simulation with 40 λ windows with each parameter (electrostatics, van der Waals, bonded) individually switched from on to off. The extremely high uncertainty observed in windows 18 \rightarrow 19 and 20 \rightarrow 21 indicates a problem with sampling due to complete decoupling of the bonds interactions, and shows that this sampling strategy does not provide a good pathway between initial and final states.

Table 3. Three-Process Mutation from Original Compound (O) to Mutated R₂ Position, to Mutated R₂ and R₃ Position, to Triple Mutant R₂, R₃, and R₁ Compared to Mutation Performed in a Single Process^a

calculation	$\Delta G/\text{kcal mol}^{-1}$	$\Delta\Delta G/\text{kcal mol}^{-1}$	(\pm) error/kcal mol ⁻¹		
complex (1aec conf2)	-20.11	-4.15	0.22		0.26
solvent (1aec conf2)	-24.27		0.14		
complex (0 \rightarrow R2)	-15.49	-3.17	0.18	0.22	0.36
solvent (0 \rightarrow R2)	-19.79		0.13		
complex (0 \rightarrow R2 \rightarrow R3)	-1.28	-0.5	0.17	0.20	
solvent (0 \rightarrow R2 \rightarrow R3)	-1.78		0.10		
complex (0 \rightarrow R2 \rightarrow R3 \rightarrow R1)	1.18	-4.29	0.17	0.20	
solvent (0 \rightarrow R2 \rightarrow R3 \rightarrow R1)	-1.99		0.10		

^aAll simulations use the replica exchange method.

exchanges by traveling back and forth between coupled and decoupled states. Increased replica exchange frequency²⁰ and multiple replica swaps per replica iteration⁴³ could significantly improve the movement of replicas between states. Additionally, the states may not be ideally aligned for configurational sampling. In the case of particle insertion, if we look at the volume with Lennard-Jones energy greater than 2 kT, ignoring the attractive $1/r^6$ term we can work out that when λ_{vdW} is

0.325 (in λ window 15) the volume of the atoms comprising the Phe-Trp-ⁱPr side chains with energy greater than 2 kT is still 76% of the equivalent volume in the fully coupled state. This large fractional excluded volume means that it is still very unlikely that the side chains could rotate easily, and more intermediate states with smaller λ_{vdW} or readjusted spacing between existing states could significantly improve the sampling using H-REMD. This hypothesis suggests that the difference in

Table 4. Free Energies Calculated for Performing the Same Single-Process Mutation for 1aec (Conformation 2) to the Reference State for Both an H-REMD Simulation and a Non-H-REMD Simulation, Indicating Close Agreement between H-REMD and Non-H-REMD Methodologies

ligand 1aec, conformation 2	$\Delta G/\text{kcal mol}^{-1}$
complex, H-REMD	-20.11 ± 0.22
solvent, H-REMD	-24.27 ± 0.14
complex, non-H-REMD	-20.30 ± 0.12
solvent, non-H-REMD	-24.90 ± 0.07

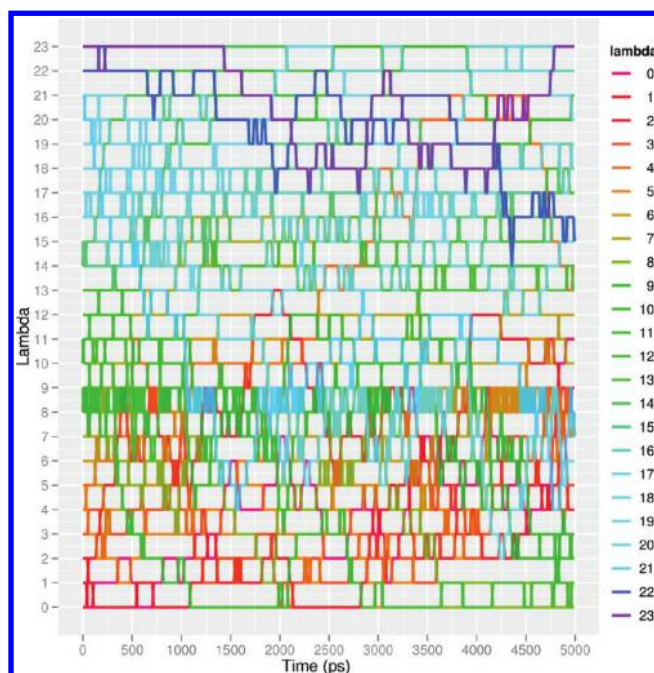


Figure 10. Hamiltonian exchange swaps over time (5 ns). Initial replicas are labeled on the y-axis and are colored consistently throughout the simulation. Swaps between neighbors are attempted every 12 ps.

accuracy must primarily be due to the slow equilibration of degrees of freedom in the simulation of the complex.

Overlap Integrals. Overlap integrals (described in Experimental Methods, subsection Overlap Integrals) allow us to investigate how close in phase space two adjacent λ windows are. The overlap in phase space is directly related to how well the H-REMD samples, since a higher overlap integral indicates that exchange between two λ windows is more likely. In Figure 11 we compared the overlap integrals for solvent simulations using a single starting conformation (starting conformation 2) of the 1aec arylamide. In the subsection Single Mutations versus Multiple Mutations we showed that the solvent simulations are converged and in statistical agreement. Therefore, we used these simulations to analyze the overlap integrals. Importantly, as hypothesized, we observe the same qualitative results are obtained for the ligand–protein complex simulations as well (see Supporting Information, Figure S1 and Table S4).

The most striking result from Figure 11 (and Supporting Information, Table S5) is that the overlap integrals from the non-H-REMD simulations appear to be considerably larger than those from the H-REMD simulations. This seems surprising, given that the thermodynamics of both systems

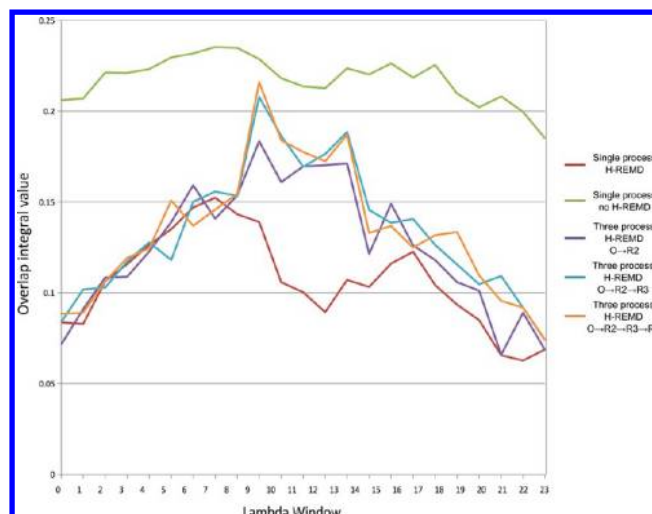


Figure 11. Overlap integrals for the H-REMD, no H-REMD and three single-process mutations for the simulations of the arylamide in solution (conformer 2 of compound 1aec). Overlap integrals for the complex are very nearly the same, and presented in Table S5 and Figure 1 of the Supporting Information.

are the same; thus, the overlap should be independent of whether the simulation uses H-REMD or not. In the subsection Hamiltonian Exchange versus Uncoupled Long Time Scale Simulations, we showed that the free energy calculations for H-REMD and non-H-REMD calculations are in agreement, showing that the thermodynamics are indeed the same. We hypothesize that the difference in the overlap integrals is due to worse sampling by the non-H-REMD simulations. Worse sampling means that similar configurations are visited more often because the systems have not yet had time to sample well, resulting in a less thorough exploration of phase space. On the basis of this data, we hypothesize that the convergence of the overlap integral appears to be a useful way to check convergence of a pair of simulations irrespective of sample size, though further tests need to be performed to observe the eventual convergence of this quantity for longer times in both H-REMD and non-H-REMD simulations.

When comparing the average overlap between the three processes and the single-process replica exchange simulations, we observe that the overlap nearer to the end points is smaller in all cases. Figure 11 shows that in the range $0 < \lambda < 9$ and $16 < \lambda < 23$, the overlap is very similar whether performing the single-process or three-process mutations. However, in the region between $9 < \lambda < 16$, we see a much larger discrepancy between the single-process and the three-process mutations. When moving from $\lambda = 12$ to $\lambda = 13$ the overlap is 0.089 for the single-process mutation compared to 0.172 for the $O \rightarrow R2 \rightarrow R3 \rightarrow R1$ part of the triple mutation. Therefore, the overlap integral is nearly twice as large for a single stage of the three-process mutation. These few states, which involve the turning off the van der Waals interaction, are the limiting factor in the one-step process; the other stages have equal overlap whether they are performed by mutating one side chain or all three. This suggests that efficient simulations can be performed by mutating multiple sites simultaneously as long as sufficiently low spacing is used in the bottleneck states.

Determining Best Binding Arylamides. Relative binding free energies for each of the compounds in Figure 1 to the reference structure using the H-REMD simulation trajectories

starting from each of the generated initial conformations were calculated using BAR and are presented in full in the Supporting Information, Table S3. The anisotropic dispersion correction was applied to simulations, and is detailed in the Experimental Methods section. The number of mutated atoms which are present in the A state but absent in the B state is also included ("mutated out" atoms). Results from simulations of each of the three starting conformations of arylamide compounds bound to *h*DM2 are combined using the exponential summation method detailed in the Experimental Methods.¹⁴ Results are also categorized by whether they are a parallel or antiparallel conformation as our previous docking and molecular dynamics simulations were unable to distinguish whether the arylamide compounds adopt a parallel or antiparallel conformation.⁸

We observe that application of the anisotropic dispersion correction significantly improves the correlation of calculated $\Delta\Delta G$ values when compared to approximate binding affinities approximated from experimentally determined IC_{50} values. Since K_d values are not available, we approximate the binding affinity by $\Delta G = -RT \ln(IC_{50})$. While it is not strictly correct to convert IC_{50} values into binding energies, in the absence of K_d values it is the only option, and since the values are all calculated in the same lab using the same experimental technique it is reasonable to assume quantitative comparisons of the differences between measurements can be made. The results from full Lennard-Jones interactions including the anisotropic dispersion correction, and those with truncated Lennard-Jones interactions, not including the anisotropic dispersion correction, correlate well with the experimental values previously published by Plante et al.¹ The full Lennard-Jones interactions appear to correlate better than the truncated Lennard-Jones interaction results ($R^2 = 0.39$ versus $R^2 = 0.13$). However, R^2 is not a particularly useful metric when the error in R^2 is large due to a small number of data points used to determine R^2 . In this case, the variance around the mean is equivalent to the variance around the fitted line, so no possible linear fit can explain much of the variance. In this case, a better measure of the success of our calculations may be the rmsd of $\Delta\Delta G$ from the experimental binding energies, which is 1.4 kcal mol⁻¹ with the anisotropic dispersion correction applied, compared to 1.3 kcal mol⁻¹ without this correction. The anisotropic dispersion correction makes little difference in the case of the smaller side chains of compounds 1acc and 1bca, but can affect the results by up to 0.5 kcal mol⁻¹ in the case of the larger side chains from compounds 1aec, 1ace, and 1acd.

The free energy of binding of parallel conformations is somewhat less favorable than the antiparallel conformations in four of the five compounds, with differences ranging from 0.7 to 1.8 kcal mol⁻¹. This is still within the statistical noise of the method, but may suggest that antiparallel binding may be preferred to parallel binding. These calculations certainly indicate that antiparallel conformations need to be considered in addition to parallel conformations when considering the binding of arylamide helix mimetics to proteins.

DISCUSSION

Results presented in the section on docking arylamide compounds to *h*DM2 showed that only the lowest energy docking solution could rank the compounds according to binding affinity using the Autodock scoring function, albeit with a slope with nonphysical magnitude of 2. It is not clear that these correlations have significant statistical significance because

of the results of the other docking-based measures of binding affinity. The Autodock scoring function has previously been reported with a standard error of approximately 2.63 kcal/mol for binding energy predictions on a set of 188 protein–ligand complexes, suggesting that the correlation is likely spurious.³⁷

We also have refined the methodology for converging the distribution of highly flexible ligands such as the arylamides. In Figure 5 we showed that the two scoring function distributions generated when using 600 and 300 conformations with enhanced sampling parameters are nearly the same, and therefore it is reasonable to use 300 conformations for the remaining five compounds. The use of 300 conformations means that the conformational degrees of freedom from the highly flexible arylamide compounds are sufficiently well sampled, leading to reproducible docked structures. We have shown that the docking methods for the highly flexible arylamide compounds with large numbers of rotatable bonds require a 10-fold increase in the number of energy evaluations, and nearly 3-fold increase in the number of genetic algorithm generations considered compared to parameters that are standard for traditional small-molecule systems.

When performing alchemical free energy calculations, we confirmed that the default placement of λ windows implemented in Desmond balance well the statistical error for the total simulation for this system. Since the total error for the simulation is most affected by the maximum error for a pair of λ values, it is desirable to spread λ values such that statistical errors are all of similar magnitude.⁴⁴

However, increasing the number λ windows may not always be desirable if the placement of these windows is not optimal (Figure 9b). It is clear from the large variance observed in λ windows 19 and 21 in Figure 9b that the individual switching methodology has some sampling problems when bonded interactions are turned off and then on, and thus one can reduce the estimated variance of the BAR calculation by using the sampling strategy shown in Table 1 and Table S2 in the Supporting Information.

It is likely that longer simulations are required to allow the calculations of the complex to better converge. The solvent simulation appears to be relatively well converged, indicated by the fact that the solvent calculations differ by only 0.7 kcal mol⁻¹ between the very different single-process and three-process mutations. We know that the dihedral angles sampled in the complex calculation may not all be well sampled in 5 ns simulations because several did not undergo transitions in the 20 ns time scale in a previous study of this system.⁸

For initial simulations comparing the performance of free energy calculations using the single-process and three-process mutations, we performed the calculations using the same single starting conformation. Thus, we expect that it is relatively unlikely for all the relevant degrees of freedom to have been sampled. We therefore chose to pursue a calculation strategy using multiple starting conformations for the rest of the calculations presented in this paper. We find a 4 kcal mol⁻¹ difference between the solvent and complex states of compound 1aec (see Supporting Information, Table S3) when using multiple starting conformations and the single-process mutation. When using multiple starting conformations to calculate the binding free energy using the single-process mutation strategy, we observe a consensus value close to 4 kcal mol⁻¹ (see Table 3), suggesting that these calculations are better converged than the triple process mutation strategy.

Our analysis of the overlap integrals from calculations on the Iaec compound (Figure 11 and Table S4 in the Supporting Information) shows that for 16 out of the 23 transitions between λ windows it is equally efficient to perform a single large mutation as to perform three steps of smaller mutations that lead to the same chemical state. These results show that performing a large single mutation can be more computationally efficient than performing several smaller mutations sequentially if proper intermediate states are selected. This novel finding is likely to benefit researchers investigating compounds with similar scaffolds or backbones but a diverse range of attachment points and functional groups such as those being investigated as helix mimetics.

The replica exchange method has known sampling benefits such as the increased likelihood of sampling dihedral angles that might otherwise be poorly sampled.^{20–31} However, we do not observe individual replicas readily transitioning between all λ states, and therefore the expected performance benefit is not fully realized. Figure 10 shows that, while the placement of λ windows has been optimized to minimize statistical error, this does not sufficiently encourage transition between all λ states within 5 ns. This novel result suggests that the minimum variance and the maximum rate of exchange may not be equal, but that the overlap is proportional to the exchange rate due to the minimal overlap and minimal exchange rate occurring in the same λ windows.

Applying anisotropic long-range dispersion corrections to the calculations in our system results in better agreement (R^2 0.39 versus R^2 0.13) with the experimentally determined free energies. Furthermore, it shows that a systematic cutoff-dependent error is introduced by ignoring the dispersion correction, as mutations involving large side chains will always tend to be underestimated. Such a systematic error is an important consideration when free energy calculations are applied to computational alanine-scanning experiments, especially when mutating a variety of larger amino acids such as tryptophan. Our anisotropic dispersion correction calculations agree with previous results on the magnitude of the effect of short vdW cutoffs over a range of (5.5–10 Å).¹⁹

When calculating alchemical free energies, we have reported the statistical error computed by bootstrap sampling of the Bennett acceptance ratio (BAR).⁴¹ The error that we report is the statistical error assuming even configuration phase sampling and should be equivalent to the sample error if the simulation were run multiple times over the same phase space.⁴⁵

CONCLUSIONS

To generate starting conformations for the arylamide compounds, we required an order of magnitude more energy evaluations and more than twice as many genetic algorithm generations than the default Autodock settings to generate consistently repeatable results. We observed that the lowest Autodock score showed strong correlation of the relative rank of compounds. However, two alternative measures, Autodock score of the largest low-energy cluster (previously shown to be more accurate than lowest energy searches⁴²) and exponentially averaged Autodock scores, showed weak or no correlation. This indicates that one must be cautious in using binding affinities calculated from Autodock scores in the case of the arylamide compounds and potentially other flexible compounds.

Converged free energy calculations for a specific mutation should yield the same result independent of the pathway taken, and the difference of 3.8 kcal mol^{−1} between the two

thermodynamic cycles for the single process and triple process mutations shows that one or both of the calculations is not converged. Performing the triple mutation shows benefits over performing the three single mutations because for 16 out of the 23 transitions between λ windows the overlap integral was comparable in magnitude to the transformations performed with single mutations. This means that for most of the transitions performing the triple mutant was roughly three times as efficient, and additional states are required to improve the overlap for only a small number of transitions. Performing the calculation as a single process could allow nearly three times as much simulation given fixed resources, allowing the opportunity to sample long time scale motions such as correlated dihedral motions. This scaling might extend to additional numbers of side chains. Additionally, if a prepared system takes significant simulation time to relax into an equilibrium state, then the effective sampling time of shorter simulations is greatly reduced, providing a significantly greater advantage for a multiple mutant simulation which can be conducted for longer time using the same computational power.

Our results strongly suggest that the sampling of states with H-REMD is better than those without H-REMD, since results from H-REMD calculations with different starting conformations produced free energies that agree to within 1.5 kcal mol^{−1}. However, Hamiltonian replica exchange may not be substantially improving sampling for the most important long time scale degrees of freedom such as dihedral angles in the arylamide and the hDM2 binding site. The Hamiltonian replica exchange procedure presented here can presumably be improved by placing additional intermediate states maximizing the overlap in phase space and by increasing the frequency that exchanges are attempted.^{20,30} Better λ placement and increased swap frequency would increase the probability of transitioning between λ states.^{20,30} The use of the overlap integral to guide placement of λ windows may be a straightforward way to approach the problem of efficient λ window placement for not only variance reduction but for improved replica exchange efficiency, though further research will be required to determine if it is reliable.

Our calculations show that there is a difference of up to 1.1 kcal mol^{−1} between the affinities calculated for parallel and those calculated from antiparallel conformations. The relatively small apparent difference in binding energy between the antiparallel and parallel conformations means that design efforts should consider both possible conformations in further arylamide rational design of better inhibitors of the hDM2–p53 interaction as either conformation may become more dominant as the side chains are changed.

The results from the free energy calculations presented here correspond well (within 1.4 kcal mol^{−1}) with the experimental data currently available. In aggregate, 1.4 kcal mol^{−1} is enough to bias selection toward tight binders.⁴³ Better validation of the method would be possible with a larger range of binding affinities of arylamide compounds, ideally with some affinities being in the nM range, but such compounds do not currently exist. Traditional approaches to free energy calculations have favored small alchemical changes. Our calculations suggest that it may be significantly more efficient to perform longer simulations while using the same computer resources by making larger alchemical changes.

■ ASSOCIATED CONTENT

■ Supporting Information

Tables describing the placement of λ states in the 12 λ window and 40 λ window simulations, results from free energy calculations and results showing the calculated overlap integrals are including in an accompanying PDF document. PDB coordinates of the docked arylamide conformations used are included in a supporting zip file. This material is available free of charge via the Internet at <http://pubs.acs.org>.

■ AUTHOR INFORMATION

Corresponding Author

*E-mail: michael.shirts@virginia.edu.

Present Address

[§]Heidelberg Institute for Theoretical Studies, Schloss-Wolf-sbrunnenweg 35, 69118 Heidelberg, Germany.

Notes

The authors declare no competing financial interest.

■ ACKNOWLEDGMENTS

We thank the Biotechnology and Biological Sciences Research Council (BBSRC) for funding J.C.F. in the form of a Ph.D. studentship and the Collaborative Computational Project for Biomolecular Simulation (CCPB) in the form of a USPA Travel award for visiting the USA. We thank Andrew J. Wilson and Thomas A. Edwards for introducing us to the *hDM2*–arylamine system. We thank Istvan Kolosvary for assistance in setting up the Desmond input files. We thank Jeff Wereszczynski for providing the full GAFF force field parameter set for use with Desmond. We thank Mark Dixon for assistance in running Desmond on the ARC computer cluster at the University of Leeds.

■ REFERENCES

- (1) Plante, J. P.; Burnley, T.; Malkova, B.; Webb, M. E.; Warriner, S. L.; Edwards, T. A.; Wilson, A. J. *Chem. Commun. (Cambridge)* **2009**, 5091–3.
- (2) Dickens, M. P.; Fitzgerald, R.; Fischer, P. M. *Semin. Cancer Biol.* **2010**, 20, 10–8.
- (3) Gellman, S. H. *Acc. Chem. Res.* **1998**, 31, 173–180.
- (4) Hill, D. J.; Mio, M. J.; Prince, R. B.; Hughes, T. S.; Moore, J. S. *Chem. Rev.* **2001**, 101, 3893–4012.
- (5) Vazquez, A.; Bond, E. E.; Levine, A. J.; Bond, G. L. *Nat. Rev. Drug Discov.* **2008**, 7, 979–87.
- (6) Warren, G. L.; Andrews, C. W.; Capelli, A.-M.; Clarke, B.; LaLonde, J.; Lambert, M. H.; Lindvall, M.; Nevins, N.; Semus, S. F.; Senger, S.; Tedesco, G.; Wall, I. D.; Woolven, J. M.; Peishoff, C. E.; Head, M. S. *J. Med. Chem.* **2006**, 49, 5912–31.
- (7) Shaginian, A.; Whitby, L. R.; Hong, S.; Hwang, I.; Farooqi, B.; Searcey, M.; Chen, J.; Vogt, P. K.; Boger, D. L. *J. Am. Chem. Soc.* **2009**, 131, 5564–5572.
- (8) Fuller, J. C.; Jackson, R. M.; Edwards, T. A.; Wilson, A. J.; Shirts, M. R. *PLOS One* **2012**, 7 (8), e43253.
- (9) Woo, H.-J.; Roux, B. *Proc. Natl. Acad. Sci. U.S.A.* **2005**, 102, 6825–30.
- (10) Lawrenz, M.; Wereszczynski, J.; Amaro, R.; Walker, R.; Roitberg, A.; McCammon, J. A. *Proteins* **2010**, 78, 2523–32.
- (11) Woods, C. J.; Essex, J. W.; King, M. A. *J. Phys. Chem. B* **2003**, 107, 13703–13710.
- (12) Mobley, D. L.; Bayly, C. I.; Cooper, M. D.; Shirts, M. R.; Dill, K. A. *J. Chem. Theory Comput.* **2009**, 5, 350–358.
- (13) Woods, C. J.; King, M. A.; Essex, J. W. *J. Comput. Aided Mol. Des.* **2001**, 15, 129–44.
- (14) Deng, Y.; Roux, B. *J. Phys. Chem. B* **2009**, 113, 2234–46.
- (15) Bruckner, S.; Boresch, S. *J. Comput. Chem.* **2011**, 32, 1303–19.
- (16) Hritz, J.; Oostenbrink, C. *J. Phys. Chem. B* **2009**, 113, 12711–20.
- (17) Mobley, D. L.; Dumont, E.; Chodera, J. D.; Dill, K. A. *J. Phys. Chem. B* **2007**, 111, 2242–54.
- (18) Shirts, M. R.; Pande, V. S. *J. Chem. Phys.* **2005**, 122, 134508.
- (19) Shirts, M. R.; Mobley, D. L.; Chodera, J. D.; Pande, V. S. *J. Phys. Chem. B* **2007**, 111, 13052–63.
- (20) Sindhikara, D.; Meng, Y.; Roitberg, A. E. *J. Chem. Phys.* **2008**, 128, 024103.
- (21) Hansmann, U. H. E. *Chem. Phys. Lett.* **1997**, 281, 140–150.
- (22) Sugita, Y.; Okamoto, Y. *Chem. Phys. Lett.* **1999**, 314, 141–151.
- (23) Denschlag, R.; Lingenehl, M.; Tavan, P. *Chem. Phys. Lett.* **2008**, 458, 244–248.
- (24) Sugita, Y.; Kitao, A.; Okamoto, Y. *J. Chem. Phys.* **2000**, 113, 6042.
- (25) Fukunishi, H.; Watanabe, O.; Takada, S. *J. Chem. Phys.* **2002**, 116, 9058.
- (26) Rosta, E.; Hummer, G. *J. Chem. Phys.* **2009**, 131, 165102.
- (27) Rosta, E.; Hummer, G. *J. Chem. Phys.* **2010**, 132, 034102.
- (28) Zuckerman, D. M.; Lyman, E. J. *Chem. Theory Comput.* **2006**, 2, 1200–1202.
- (29) Nymeyer, H. *J. Chem. Theory Comput.* **2008**, 4, 626–636.
- (30) Sindhikara, D. J.; Emerson, D. J.; Roitberg, A. E. *J. Chem. Theory Comput.* **2010**, 6, 2804–2808.
- (31) Cossins, B. P.; Foucher, S.; Edge, C. M.; Essex, J. W. *J. Phys. Chem. B* **2009**, 113, 5508–19.
- (32) Paluch, A. S.; Mobley, D. L.; Maginn, E. J. *J. Chem. Theory Comput.* **2011**, 7, 2910–2918.
- (33) Bowers, K. J.; Sacerdoti, F. D.; Salmon, J. K.; Shan, Y.; Shaw, D. E.; Chow, E.; Xu, H.; Dror, R. O.; Eastwood, M. P.; Gregersen, B. A.; Klepeis, J. L.; Kolosvary, I.; Moraes, M. A. *Molecular Dynamics—Scalable Algorithms for Molecular Dynamics Simulations on Commodity Clusters*; ACM Press: New York, 2006; p 84.
- (34) Michel, J.; Harker, E. A.; Tirado-Rives, J.; Jorgensen, W. L.; Schepartz, A. *J. Am. Chem. Soc.* **2009**, 131, 6356–7.
- (35) Mobley, D. L.; Chodera, J. D.; Dill, K. A. *J. Chem. Phys.* **2006**, 125, 084902.
- (36) Morris, G. M.; Goodsell, D. S.; Halliday, R. S.; Huey, R.; Hart, W. E.; Belew, R. K.; Olson, A. J. *J. Comput. Chem.* **1998**, 19, 1639–1662.
- (37) Huey, R.; Morris, G. M.; Olson, A. J.; Goodsell, D. S. *J. Comput. Chem.* **2007**, 28, 1145–52.
- (38) Martyna, G. J.; Tobias, D. J.; Klein, M. L. *J. Chem. Phys.* **1994**, 101, 4177.
- (39) Esposito, M.; Monnai, T. *J. Phys. Chem. B* **2010**.
- (40) Pham, T. T.; Shirts, M. R. *J. Chem. Phys.* **2011**, 135, 034114.
- (41) Bennett, C. *J. Comput. Phys.* **1976**, 22, 245–268.
- (42) Illingworth, C. J. R.; Morris, G. M.; Parkes, K. E. B.; Snell, C. R.; Reynolds, C. A. *J. Phys. Chem. A* **2008**, 112, 12157–63.
- (43) Shirts, M. R.; Mobley, D. L.; Chodera, J. D. *Annu. Rep. Comput. Chem.* **2007**, 3, 41–59.
- (44) Shenfeld, D.; Xu, H.; Eastwood, M.; Dror, R.; Shaw, D. *Phys. Rev. E* **2009**, 80, 1–4.
- (45) Paliwal, H.; Shirts, M. R. *J. Chem. Theory Comput.* **2011**, 7, 4115–4134.